Search in the Two-Photon Final State for Evidence of New Particle Production at the Large Hadron Collider

Rachel P. Yohay

University of Virginia

rpy3y@virginia.edu

January 15, 2012

Contents

Chapter 1

The Supersymmetric Extension to the Standard Model

The following introduction to SUSY focuses primarily on the aspects of the formalism that are relevant to phenomenology. In particular, most of the details of SUSY breaking (about which there is little theoretical consensus) are omitted, except where they are relevant to experiment. The notation is similar to that used in refs. [18] and [5].

1.1 Supermultiplet Representation

The Standard Model is extended to include supersymmetry by the introduction of a supersymmetry transformation that takes fermionic states to bosonic states and vice versa. The resulting model is called the *minimal supersymmetric Standard Model* (MSSM). In analogy with the known symmetries of the Standard Model, the SUSY transformation has associated generators that obey defining commutation relations, and a fundamental representation. All SM particles and their *superpartners* fall into one of two *supermultiplet* representations. Using the property that

$$n_F = n_B, \tag{1.1}$$

where n_F is the number of fermionic degrees of freedom per supermultiplet and n_B is the number of bosonic degrees of freedom, the two types of supermultiplets are

1. *Chiral supermultiplets*: one Weyl fermion (two helicity states $\Rightarrow n_F = 2$) and one complex scalar field (with two real components $\Rightarrow n_B = 2$)

2. *Gauge supermultiplets*: One spin-1 vector boson (two helicity states $\Rightarrow n_B = 2$) and one Weyl fermion (two helicity states $\Rightarrow n_F = 2$)

In the gauge supermultiplet, the vector boson is assumed massless (i.e. before EWSB generates a mass for it). Since the superpartners to the SM particles have not yet been discovered, they must be significantly heavier than their SM counterparts. Unbroken SUSY predicts that the SM particles and their superpartners must have exactly the same mass, so ultimately a mechanism for SUSY breaking must be introduced to generate masses for the superpartners (see Sec. 1.3). Tables 1.1 and 1.2 show the chiral and gauge supermultiplets of the MSSM, respectively. Note that the scalar partners to the SM fermions are denoted by placing an "s" in front of their names, while the chiral fermion partners to the SM gauge bosons are denoted by appending "ino" to their names.

1.2 The Unbroken SUSY Lagrangian

The first piece of the full unbroken SUSY Lagrangian density consists of the kinetic and interacting terms related to the chiral supermultiplets. As explained in Sec. 1.1, a chiral supermultiplet consists of a Weyl fermion ψ (the ordinary fermion) and a complex scalar ϕ (the sfermion). For a collection of such chiral supermultiplets, the Lagrangian is

Table 1.1: Chiral supermultiplets of the supersymmetric Standard Model. Adapted from Table 1.1 of ref. [18].

Type of supermultiplet	Notation	Spin-0 component	Spin-1/2 component	Representation under $SU(3)_C \otimes SU(2)_L \otimes U(1)_Y$
Left-handed quark/squark doublet ($\times$ 3 families)	Q	$(\widetilde{u}_L\ \widetilde{d}_L)$	$(u_L\ d_L)$	$(\mathbf{3},\ \mathbf{2},\ \frac{1}{6})$
Right-handed up-type quark/squark singlet ($\times$ 3 families)	$\overline{u}$	$\widetilde{u}_R^*$	$u_R^\dagger$	$(\overline{\mathbf{3}},\ \mathbf{1},\ -\frac{2}{3})$
Right-handed down-type quark/squark singlet ($\times$ 3 families)	$\overline{d}$	$\widetilde{d}_R^*$	$d_R^\dagger$	$(\overline{\mathbf{3}},\ \mathbf{1},\ \frac{1}{3})$
Left-handed lepton/slepton doublet ($\times$ 3 families)	L	$(\widetilde{\overline{\nu}}_{eL}\ \widetilde{e}_L)$	$(\overline{\nu}_{eL}\ e_L)$	$(\mathbf{1},\ \mathbf{2},\ -\frac{1}{2})$
Right-handed lepton/slepton singlet ($\times$ 3 families)	$\overline{e}$	$\widetilde{e}_R^*$	$e_R^\dagger$	$(\overline{\mathbf{1}},\ \mathbf{1},\ 1)$
Up-type Higgs/Higgsino doublet	H_u	$(H_u^+\ H_u^0)$	$(\widetilde{H}_u^+\ \widetilde{H}_u^0)$	$(\mathbf{1},\ \mathbf{2},\ \frac{1}{2})$
Down-type Higgs/Higgsino doublet	H_d	$(H_d^0\ H_d^-)$	$(\widetilde{H}_d^0\ \widetilde{H}_d^-)$	$(\mathbf{1},\ \mathbf{2},\ -\frac{1}{2})$

Table 1.2: Gauge supermultiplets of the supersymmetric Standard Model. Adapted from Table 1.2 of ref. [18].

Type of supermultiplet	Spin-1/2 component	Spin-1 component	Representation under $SU(3)_C \otimes SU(2)_L \otimes U(1)_Y$
Gluon/gluino	$\widetilde{g}$	g	$(\mathbf{8},\ \mathbf{1},\ 0)$
W/wino	$\widetilde{W}^\pm\ \widetilde{W}^0$	$W^\pm\ W^0$	$(\mathbf{1},\ \mathbf{3},\ 0)$
B/bino	$\widetilde{B}^0$	B^0	$(\mathbf{1},\ \mathbf{1},\ 0)$

$$\begin{aligned}\mathcal{L}_{\rm chiral} &= -\partial^\mu \phi^{*i} \partial_\mu \phi_i \; - \; V_{\rm chiral}(\phi, \phi^*) \; - \; i\psi^{\dagger i} \overline{\sigma}^\mu \partial_\mu \psi_i \; - \; \frac{1}{2} M^{ij} \psi_i \psi_j \\ &\quad - \frac{1}{2} M^*_{ij} \psi^{\dagger i} \psi^{\dagger j} \; - \; \frac{1}{2} y^{ijk} \phi_i \psi_j \psi_k \; - \; \frac{1}{2} y^*_{ijk} \phi^{*i} \psi^{\dagger j} \psi^{\dagger k} \end{aligned} \tag{1.2}$$

where i runs over all supermultiplets in Table 1.1, $\overline{\sigma}^\mu$ are -1 $\times$ the Pauli matrices (except for $\sigma^0 = \overline{\sigma}^0$), M^{ij} is a mass matrix for the fermions, y^{ijk} are the Yukawa couplings between one scalar and two spinor fields, and $V_{\rm chiral}(\phi, \phi^*)$ is the scalar potential

$$\begin{aligned} V_{\rm chiral}(\phi, \phi^*) &= M^*_{ik} M^{kj} \phi^{*i} \phi_j \; + \; \frac{1}{2} M^{in} y^*_{jkn} \phi_i \phi^{*j} \phi^{*k} \\ &\quad + \frac{1}{2} M^*_{in} y^{jkn} \phi^{*i} \phi_j \phi_k \; + \; \frac{1}{4} y^{ijn} y^*_{kln} \phi_i \phi_j \phi^{*k} \phi^{*l}. \end{aligned} \tag{1.3}$$

The Lagrangian can also be written as the kinetic terms plus derivatives of the *superpotential* W:

$$\begin{aligned}\mathcal{L}_{\rm chiral} &= -\partial^\mu \phi^{*i} \partial_\mu \phi_i \; - \; i\psi^{\dagger i} \overline{\sigma}^\mu \partial_\mu \psi_i \\ &\quad - \frac{1}{2} \left(\frac{\delta^2 W}{\delta \phi^i \delta \phi^j} \psi_i \psi_j + \frac{\delta^2 W^*}{\delta \phi_i \delta \phi_j} \psi^{\dagger i} \psi^{\dagger j} \right) \; - \; \frac{\delta W}{\delta \phi^i} \frac{\delta W^*}{\delta \phi_i} \end{aligned} \tag{1.4}$$

where

$$W \;=\; M^{ij} \phi_i \phi_j \; + \; \frac{1}{6} y^{ijk} \phi_i \phi_j \phi_k. \tag{1.5}$$

The second part of the Lagrangian involves the gauge supermultiplets. In terms of the spin-1 ordinary gauge boson A^a_μ and the spin-1/2 Weyl spinor gaugino λ^a of

the gauge supermultiplet, where a runs over the number of generators for the SM subgroup (i.e. 1-8 for $SU(3)_C$, 1-3 for $SU(2)_L$, and 1 for $U(1)_Y$), this part of the Lagrangian is

$$\mathcal{L}_{\text{gauge}} \;=\; -\frac{1}{4}F^a_{\mu\nu}F^{\mu\nu a} \;-\; i\lambda^{\dagger a}\overline{\sigma}^\mu D_\mu\lambda^a \;+\; \frac{1}{2}D^aD^a \tag{1.6}$$

where

$$F^a_{\mu\nu} \;=\; \partial_\mu A^a_\nu \;-\; \partial_\nu A^a_\mu \;+\; gf^{abc}A^b_\mu A^c_\nu \tag{1.7}$$

(g is the coupling constant and f^{abc} are the structure constants for the particular SM gauge group),

$$D_\mu\lambda^a \;=\; \partial_\mu\lambda^a \;+\; gf^{abc}A^b_\mu\lambda^c, \tag{1.8}$$

and D^a is an auxiliary field that does not propagate (in the literature, it is used as a bookkeeping tool and can be removed via its algebraic equation of motion).

To build a fully supersymmetric and gauge-invariant Lagrangian, the ordinary derivatives in $\mathcal{L}_{\text{chiral}}$ (Eq. 1.2) must be replaced by covariant derivatives

$$D_\mu\phi_i \;=\; \partial_\mu\phi_i \;-\; igA^a_\mu(T^a\phi)_i \tag{1.9}$$

$$D_\mu\phi^{*i} \;=\; \partial_\mu\phi^{*i} \;+\; igA^a_\mu(\phi^*T^a)^i \tag{1.10}$$

$$D_\mu\psi_i \;=\; \partial_\mu\psi_i \;-\; igA^a_\mu(T^a\psi)_i. \tag{1.11}$$

This leads to the full Lagrangian

$$
\begin{aligned}
\mathcal{L} &= \mathcal{L}_{\text{chiral}} + \mathcal{L}_{\text{gauge}} \\
&\quad - \sqrt{2}g(\phi^{*i}T^a\psi_i)\lambda^a - \sqrt{2}g\lambda^{\dagger a}(\psi^{\dagger i}T^a\phi_i) + g(\phi^{*i}T^a\phi_i)D^a \\
&= -\partial^\mu\phi^{*i}\partial_\mu\phi_i - i\psi^{\dagger i}\overline{\sigma}^\mu\partial_\mu\psi_i + ig\partial^\mu\phi^{*i}A^a_\mu(T^a\phi)_i - ig\partial_\mu\phi_i A^{\mu a}(\phi^*T^a)^i \\
&\quad - g^2A^{\mu a}(\phi^*T^a)^iA^a_\mu(T^a\phi)_i - g\psi^{\dagger i}\overline{\sigma}^\mu A^a_\mu(T^a\psi)_i - V_{\text{chiral}}(\phi,\phi^*) \\
&\quad - \frac{1}{2}M^{ij}\psi_i\psi_j - \frac{1}{2}M^*_{ij}\psi^{\dagger i}\psi^{\dagger j} - \frac{1}{2}y^{ijk}\phi_i\psi_j\psi_k - \frac{1}{2}y^*_{ijk}\phi^{*i}\psi^{\dagger j}\psi^{\dagger k} \\
&\quad - \frac{1}{4}F^a_{\mu\nu}F^{\mu\nu a} - i\lambda^{\dagger a}\overline{\sigma}^\mu\partial_\mu\lambda^a - ig\lambda^{\dagger a}\overline{\sigma}^\mu f^{abc}A^b_\mu\lambda^c + \frac{1}{2}D^aD^a \\
&\quad - \sqrt{2}g(\phi^{*i}T^a\psi_i)\lambda^a - \sqrt{2}g\lambda^{\dagger a}(\psi^{\dagger i}T^a\phi_i) + g(\phi^{*i}T^a\phi_i)D^a. \qquad (1.12)
\end{aligned}
$$

Writing out $F^a_{\mu\nu}$ and $V_{\text{chiral}}(\phi,\phi^*)$ explicitly combining the D^a terms using the equation of motion $D^a = -g\phi^{*i}T^a\phi_i$, and rearranging some terms, the final unbroken SUSY Lagrangian is

$$
\begin{aligned}
\mathcal{L} \;=\; & -\partial^\mu \phi^{*i} \partial_\mu \phi_i \;-\; i\psi^{\dagger i}\overline{\sigma}^\mu \partial_\mu \psi_i \\
& - \frac{1}{4}(\partial_\mu A^a_\nu - \partial_\nu A^a_\mu)(\partial^\mu A^{\nu a} - \partial^\nu A^{\mu a}) \;-\; i\lambda^{\dagger a}\overline{\sigma}^\mu \partial_\mu \lambda^a \\
& - M^*_{ik} M^{kj} \phi^{*i} \phi_j \;-\; \frac{1}{2} M^{ij} \psi_i \psi_j \;-\; \frac{1}{2} M^*_{ij} \psi^{\dagger i} \psi^{\dagger j} \\
& + ig\partial^\mu \phi^{*i} A^a_\mu (T^a \phi)_i \;-\; ig\partial_\mu \phi_i A^{\mu a} (\phi^* T^a)^i \;-\; g\psi^{\dagger i}\overline{\sigma}^\mu A^a_\mu (T^a \psi)_i \\
& - ig\lambda^{\dagger a}\overline{\sigma}^\mu f^{abc} A^b_\mu \lambda^c \\
& - \frac{1}{4} g f^{abc}[(\partial_\mu A^a_\nu - \partial_\nu A^a_\mu) A^{\mu b} A^{\nu c} + A^b_\mu A^c_\nu (\partial^\mu A^{\nu a} - \partial^\nu A^{\mu a})] \\
& - \frac{1}{2} M^*_{in} y^{jkn} \phi^{*i} \phi_j \phi_k \;-\; \frac{1}{2} M^{in} y^*_{jkn} \phi_i \phi^{*j} \phi^{*k} \\
& - \frac{1}{2} y^{ijk} \phi_i \psi_j \psi_k \;-\; \frac{1}{2} y^*_{ijk} \phi^{*i} \psi^{\dagger j} \psi^{\dagger k} \\
& - \sqrt{2} g (\phi^{*i} T^a \psi_i) \lambda^a \;-\; \sqrt{2} g \lambda^{\dagger a} (\psi^{\dagger i} T^a \phi_i) \\
& - g^2 A^{\mu a} (\phi^* T^a)^i A^a_\mu (T^a \phi)_i \;-\; \frac{1}{4} g^2 f^{abc} A^b_\mu A^c_\nu f^{abc} A^{\mu b} A^{\nu c} \\
& - \frac{1}{4} y^{ijn} y^*_{kln} \phi_i \phi_j \phi^{*k} \phi^{*l} \;-\; \frac{1}{2} g^2 (\phi^{*i} T^a \phi_i)^2 .
\end{aligned}
\tag{1.13}
$$

The above Lagrangian applies to chiral supermultiplets interacting with one kind of gauge supermultiplet (i.e. one SM gauge group). In the general case, there are additional terms corresponding to interactions with all three SM gauge groups.

The following list gives a description of the terms in Eq. 1.13:

- First two lines: kinetic terms for the four types of fields ϕ_i, ψ_i, A^a_μ, and λ^a
- Third line: mass terms for the ϕ_i and ψ_i (see Figs. 1.1(a) and 1.1(b))
- Fourth and fifth lines: cubic couplings in which ϕ_i, ψ_i, or λ^a radiates an A^a_μ (see Figs. 1.1(c), 1.1(d), and 1.1(e))
- Sixth line: triple gauge boson couplings (see Fig. 1.1(f))
- Seventh line: triple sfermion couplings (see Fig. 1.1(g))

- Eighth line: cubic couplings in which ψ_i radiates a ϕ_i (see Fig. 1.1(h))
- Ninth line: ϕ_i-ψ_i-λ^a vertices (see Fig. 1.1(i))
- 10^{th} line: A^a_μ-A^a_μ-ϕ_i-ϕ_i and quadruple gauge boson couplings (see Figs. 1.1(j) and 1.1(k))
- 11^{th} line: ϕ_i^4 vertices (see Figs. 1.1(l) and 1.1(m))

1.3 Soft SUSY Breaking

Since quadratic divergences in sfermion masses vanish to all orders in perturbation theory in plain unbroken SUSY[18] due to the presence of gauge and Yukawa interactions with the necessary relationships between coupling constants, it is desirable that the terms that break SUSY not disturb this property. In addition, SUSY should be broken spontaneously, as electroweak symmetry is broken in the Standard Model, so that it is only made manifest at high energies. To satisfy these constraints, SUSY-breaking terms are simply added to the unbroken SUSY Lagrangian in Eq. 1.13 such that $\mathcal{L}_{\text{total}} = \mathcal{L}_{\text{unbroken}} + \mathcal{L}_{\text{breaking}}$. The coefficients of terms in $\mathcal{L}_{\text{breaking}}$ must have positive mass dimension in order not to contribute quadratically divergent loop corrections to the scalar masses (like the Higgs mass).[1] This form of SUSY breaking is called *soft*, and all coefficients of soft SUSY breaking terms are expected to be of order m_{soft} or m^2_{soft}.

[1]This point can be argued via dimensional analysis. Radiative corrections take the form Δm_S^2, where m_S is the mass of the scalar particle in question. The dimensions of Δm_S^2 are mass^2. Δm_S^2 is proportional to some coupling constant or mass coefficient k multiplied by a function of Λ_{UV}, the high energy cutoff scale. The function of Λ_{UV} is determined by a loop integral, and thus typically takes the form Λ^2_{UV} (quadratically divergent) or $\ln \frac{\Lambda_{\text{UV}}}{m_{\text{low}}}$ (logarithmically divergent, where m_{low} is some other lower-mass scale in the problem). Now, if k already contributes at least one power of mass to Δm_S^2, then the high-energy behavior—the function of Λ_{UV}—can only contribute at most one power of the dimensionful parameter Λ_{UV}. However, there are typically no loop integrals that diverge linearly in Λ_{UV}, so by forcing k to have positive mass dimension, the form of the radiative corrections contributed by SUSY-breaking terms is limited to $\Delta m_S^2 \sim m^2_{\text{low}} \ln \frac{\Lambda_{\text{UV}}}{m_{\text{low}}}$. In effect, the possibility of dangerous corrections proportional to Λ^2_{UV} is excluded by dimensional analysis if the requirement that k contribute at least one power of mass is enforced.

(a) Fermion mass terms. Reprinted from Figs. 3.2(c) and 3.2(d) of ref. [18].

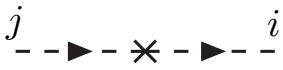

(b) Sfermion mass terms. Reprinted from Fig. 3.2(e) of ref. [18].

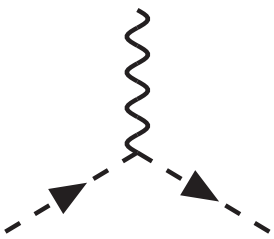

(c) $A\phi\phi$ vertex. Reprinted from Fig. 3.3(e) of ref. [18].

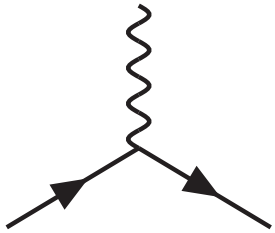

(d) $A\psi\psi$ vertex. Reprinted from Fig. 3.3(f) of ref. [18].

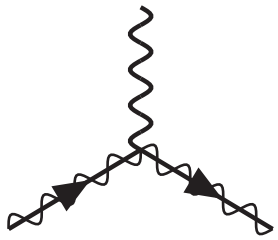

(e) $A\lambda\lambda$ vertex. Reprinted from Fig. 3.3(c) of ref. [18].

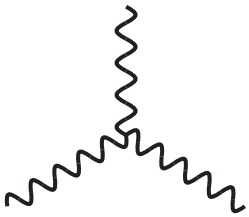

(f) Triple gauge boson vertex. Reprinted from Fig. 3.3(b) of ref. [18].

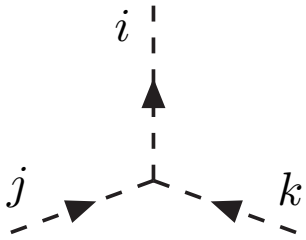

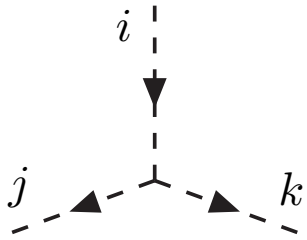

(g) Triple sfermion vertices. Reprinted from Figs. 3.2(a) and 3.2(b) of ref. [18].

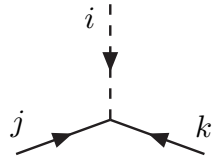

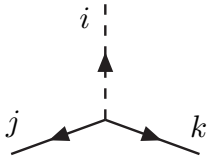

(h) Cubic couplings in which the fermion radiates a sfermion. Reprinted from Figs. 3.1(a) and 3.1(b) of ref. [18].

(i) Sfermion-fermion-gaugino vertices. Reprinted from Figs. 3.3(g) and 3.3(h) of ref. [18].

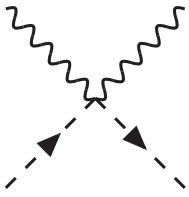

(j) $AA\phi\phi$ vertex. Reprinted from Fig. 3.3(d) of ref. [18].

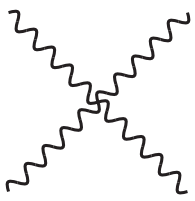

(k) Quadruple gauge boson vertex. Reprinted from Fig. 3.3(a) of ref. [18].

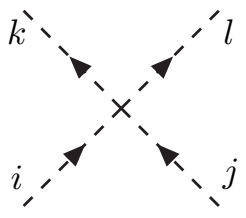

(l) Non-gauge ϕ^4 vertex. Reprinted from Fig. 3.1(c) of ref. [18].

(m) Gauge ϕ^4 vertex. Reprinted from Fig. 3.3(i) of ref. [18].

Figure 1.1: Interactions in the unbroken SUSY Lagrangian.

Soft SUSY breaking terms give masses to the sfermions and gauginos and introduce a cubic sfermion vertex. The soft terms are given by

$$\begin{aligned}
\mathcal{L}_{\text{soft}} &= -\frac{1}{2}(M_3\widetilde{g}^a\widetilde{g}^a + M_2\widetilde{W}^a\widetilde{W}^a + M_1\widetilde{B}\widetilde{B} + \text{h.c.}) \\
&\quad - (a_u^{ij}\widetilde{u}^*_{Ri}\widetilde{Q}_j H_u - a_d^{ij}\widetilde{d}^*_{Ri}\widetilde{Q}_j H_d - a_e^{ij}\widetilde{e}^*_{Ri}\widetilde{L}_j H_d + \text{h.c.}) \\
&\quad - m^2_{\widetilde{Q}ij}\widetilde{Q}_i^\dagger\widetilde{Q}_j \;-\; m^2_{\widetilde{L}ij}\widetilde{L}_i^\dagger\widetilde{L}_j \\
&\quad - m^2_{\widetilde{\bar{u}}ij}\widetilde{u}_{Ri}\widetilde{u}^*_{Rj} \;-\; m^2_{\widetilde{\bar{d}}ij}\widetilde{d}_{Ri}\widetilde{d}^*_{Rj} \;-\; m^2_{\widetilde{\bar{e}}ij}\widetilde{e}_{Ri}\widetilde{e}^*_{Rj} \\
&\quad - m^2_{H_u}H_u^* H_u \;-\; m^2_{H_d}H_d^* H_d \;-\; (bH_u H_d + \text{h.c.})
\end{aligned} \tag{1.14}$$

where a runs from 1-8 for $\widetilde{g}^a$ and from 1-3 for $\widetilde{W}^a$, and i, j run over the three families. The color indices are not shown. The first line of Eq. 1.14 contains the gaugino mass terms. The second line contains cubic scalar couplings that contribute to mixing between the left- and right-handed third generation sfermions (it is assumed in the supersymmetric Standard Model that the a_u^{ij}, a_d^{ij}, and a_e^{ij} are negligible unless $i = j = 3$). The third and fourth lines of Eq. 1.14 contain squark and slepton mass terms, and finally the last line contains the Higgs mass terms.

Many viable models of achieving soft SUSY breaking have been studied over the last 30 years. For an overview, see Sec. 6 of ref. [18]. However, this thesis will only cover *gauge-mediated SUSY breaking* (GMSB), because the two-photon search performed is far more sensitive to this model than to other models of SUSY breaking.

1.4 Gauge-Mediated SUSY Breaking

In gauge-mediated models[7],"hidden" fields spontaneously break the supersymmetry of very heavy chiral *messenger* supermultiplets. There are a number of competing models (see ref. [7]) that explain the precise mechanism of spontaneous SUSY

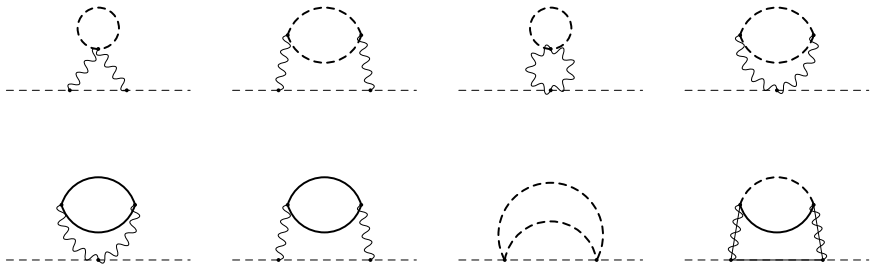

(a) Sfermion mass terms. Heavy dashed lines denote messenger sfermions; solid lines denote messenger fermions. Reprinted from Fig. 6.4 of ref. [18].

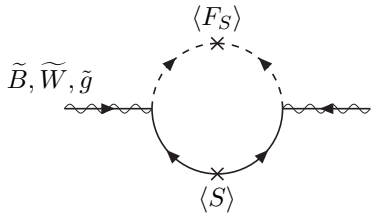

(b) Gaugino mass term. The $\langle S \rangle$ part of the loop is a messenger fermion contribution; the $\langle F_S \rangle$ part is a messenger sfermion contribution. Reprinted from Fig. 6.3 of ref. [18].

Figure 1.2: Contributions to sfermion and gaugino masses from loop interactions with messenger particles in the GMSB framework.

breaking, but fortunately the details of those models mostly decouple from the phenomenology of GMSB. The messengers then communicate the SUSY breaking to the sparticles via loop diagrams of gauge interaction strength (i.e. via vertices like those shown in Figs. 1.1(c), 1.1(d), 1.1(i), 1.1(j), and 1.1(m), which are proportional to the SM gauge couplings constants). Feynman diagrams corresponding to gaugino and sfermion mass terms are shown in Figure 1.2.

Historically, GMSB and gravity-mediated SUSY breaking, or mSUGRA[8], have been the two most thoroughly experimentally studied scenarios of SUSY breaking. One advantage of GMSB over mSUGRA is that it naturally suppresses flavor violation, a generic prediction of supersymmetry. Flavor violation is introduced in the scalar^3 couplings and sfermion mass terms of $\mathcal{L}_{\text{soft}}$ (second, third, and fourth lines of

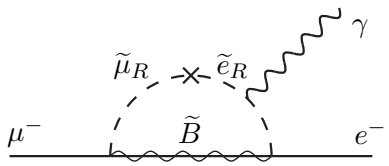

Figure 1.3: Possible contribution to $\mu \to e\gamma$ from $m^2_{\widetilde{e}ij}$ soft term. Reprinted from Fig. 5.6(a) of ref. [18].

Eq. 1.14). Since a_u^{ij}, a_d^{ij}, a_e^{ij}, $m^2_{\widetilde{Q}ij}$, $m^2_{\widetilde{L}ij}$, $m^2_{\widetilde{\overline{u}}ij}$, $m^2_{\widetilde{\overline{d}}ij}$, and $m^2_{\widetilde{\overline{e}}ij}$ are matrices in family space, any nonzero off-diagonal elements will lead to mixing between sfermions of different families. This can lead, for example, to contributions to the diagram $\mu \to e\gamma$ (Figure 1.3) exceeding the experimental bounds. To avoid this disaster, *universality* conditions are assumed:

$$\mathbf{m^2_{\widetilde{Q}}} = m^2_{\widetilde{Q}}\mathbf{1},\ \mathbf{m^2_{\widetilde{L}}} = m^2_{\widetilde{L}}\mathbf{1},\ \mathbf{m^2_{\widetilde{\overline{u}}}} = m^2_{\widetilde{\overline{u}}}\mathbf{1},\ \mathbf{m^2_{\widetilde{\overline{d}}}} = m^2_{\widetilde{\overline{d}}}\mathbf{1},\ \mathbf{m^2_{\widetilde{\overline{e}}}} = m^2_{\widetilde{\overline{e}}}\mathbf{1} \tag{1.15}$$

i.e. all sfermion mass matrices arising from the soft terms are assumed to be proportional to the unit matrix **1**, such that there can be no flavor mixing from these terms and contributions to flavor-changing processes are drastically reduced.[2] In mSUGRA models, universality is assumed from the beginning, while in GMSB it is a natural consequence of the fact that the sparticle-messenger vertices are flavor-blind.

In minimal GMSB (mGMSB), there are four messenger supermultiplets q, $\overline{q}$, l, $\overline{l}$ providing the messenger (s)quarks and (s)leptons. There is one breaking scale Λ. The gaugino masses computed from diagrams like Fig. 1.2(b) are given by

$$M_a = \frac{\alpha_a}{4\pi}\Lambda \tag{1.16}$$

[2]Universality also includes some assumptions about the form of a_{uij}, a_{dij}, and a_{eij} and the stipulation that the soft terms not introduce any CP-violating phases.

where a runs from 1-3 and the α_a are the SM gauge coupling constants. The sfermion masses computed from diagrams like Fig. 1.2(a) are given by

$$m^2_{\phi_i} = 2\Lambda^2 \sum_{a=1}^{3} (\frac{\alpha_a}{4\pi})^2 C_a(i) \tag{1.17}$$

where $C_a(i)$ are group theory factors that are identical for all particles residing in the same type of supermultiplet (e.g. for all left-handed (s)quarks or left-handed (s)leptons). As explained in the previous paragraph, the gaugino and sfermion masses do not depend on fermion family.

In recent years, much theoretical progress has been made in unifying models of gauge mediation and developing less restrictive models than mGMSB. *General gauge mediation* (GGM)[9] retains the essential features of mGMSB, such as flavor degeneracy and communication of SUSY breaking via messengers, but does not make assumptions about the specific messenger sector or SUSY breaking scale. Many different collider final states can be interpreted in terms of GGM, and conversely, GGM implies a wealth of signatures, only a small fraction of which have been searched for at colliders[10, 11, 12]. The following section discusses the aspects of GGM collider phenomenology relevant to this thesis.

1.5 Phenomenology of General Gauge Mediation

The main distinguishing feature of all GMSB phenomenology is that the gravitino $\widetilde{G}$ is very light (eV-keV). In general, the gravitino mass is proportional to $\langle F \rangle / M_P$, where $\langle F \rangle$ is the vacuum expectation value (VEV) of a field F that spontaneously breaks SUSY in the vacuum state and M_P is the Planck mass. In GGM models, $\langle F \rangle \sim 10^8$ GeV, leading to a very light gravitino. In contrast, mSUGRA predicts $\langle F \rangle \sim 10^{20}$ GeV. The fact that the gravitino is so much lighter than any other particles in the

supersymmetric Standard Model, and that it interacts only gravitationally (and thus extremely feebly), leads to two important phenomenological consequences:

1. All sparticle decay chains end with the production of a gravitino.

2. The gravitino escapes 4π, hermetic collider detectors without interacting, leaving a signature of "missing" momentum transverse to the beam direction.

Even if the gravitino were lighter than any other sparticle, but heavier than an ordinary SM particle, it still could not decay to the SM particle due to *R-parity*. R-parity is a conserved quantity of the supersymmetric Standard Model that enforces baryon and lepton number conservation, which would otherwise be generically allowed at levels in conflict with experiment (e.g. the non-observation of baryon- and lepton-number-violating proton decay). All sparticles have R-parity -1, while all ordinary SM particles have R-parity +1, and R-parity conservation dictates that at any vertex, the product of the R-parities of each leg must be +1. This leads to two more important consequences:

1. Since conservation of energy only allows it to decay to ordinary SM particles, but R-parity prevents a sparticle-particle-particle vertex, the *lightest supersymmetric particle* (LSP) must be absolutely stable. All sparticle decays proceed through the *next-to-lightest supersymmetric particle* (NLSP), which in turn decays to the LSP. The fact that it is stable and only gravitationally interacting makes the gravitino a candidate dark matter particle (see Sec. 1.6).

2. In colliders, sparticles are produced in pairs (particle + particle $\rightarrow$ sparticle + sparticle).

In GMSB, then, the gravitino is the LSP. If the NLSP is a gaugino,[3] then the possible decays depend on mixing among the gauginos. Due to the effects of EWSB,

[3]In principle, the NLSP could be anything, but in most popular GGM models, it is either a gaugino or a stau. The stau NLSP search is not the subject of this thesis, so it will not be considered in this section.

the four neutral gauginos $\widetilde{H}_u^0$, $\widetilde{H}_d^0$, $\widetilde{B}$, $\widetilde{W}^0$ mix into four *neutralino* mass eigenstates $\widetilde{\chi}_1^0, \widetilde{\chi}_2^0, \widetilde{\chi}_3^0, \widetilde{\chi}_4^0$, and the four charged gauginos $\widetilde{H}_u^+$, $\widetilde{H}_d^-$, $\widetilde{W}^+$, $\widetilde{W}^-$ mix into two *chargino* mass eigenstates $\widetilde{\chi}_1^\pm, \widetilde{\chi}_2^\pm$ (two mass eigenstates each with two possible charges = four particles). In the limit that EWSB effects are small, the neutralino and chargino masses can be written as the gauge eigenstate masses plus a small perturbation:

$$m_{\widetilde{\chi}_1^0} = M_1 - \frac{m_Z^2 \sin^2\theta_W (M_1 + \mu \sin 2\beta)}{\mu^2 - M_1^2} + ... \tag{1.18}$$

$$m_{\widetilde{\chi}_2^0} = M_2 - \frac{m_W^2 (M_2 + \mu \sin 2\beta)}{\mu^2 - M_2^2} + ... \tag{1.19}$$

$$m_{\widetilde{\chi}_3^0} = |\mu| + \frac{m_Z^2 (\mathrm{sgn}(\mu) - \sin 2\beta)(\mu + M_1 \cos^2\theta_W + M_2 \sin^2\theta_W)}{2(\mu + M_1)(\mu + M_2)} + ... \tag{1.20}$$

$$m_{\widetilde{\chi}_4^0} = |\mu| + \frac{m_Z^2 (\mathrm{sgn}(\mu) + \sin 2\beta)(\mu - M_1 \cos^2\theta_W - M_2 \sin^2\theta_W)}{2(\mu - M_1)(\mu - M_2)} + ... \tag{1.21}$$

$$m_{\widetilde{\chi}_1^\pm} = M_2 - \frac{m_W^2 (M_2 + \mu \sin 2\beta)}{\mu^2 - M_2^2} + ... \tag{1.22}$$

$$m_{\widetilde{\chi}_2^\pm} = |\mu| + \frac{m_W^2 \,\mathrm{sgn}(\mu)(\mu + M_2 \sin 2\beta)}{\mu^2 - M_2^2} + ... \tag{1.23}$$

where $\tan\beta = \langle H_u^0 \rangle / \langle H_d^0 \rangle$.

The two scenarios studied in ref. [12] are the following:

- **Bino NLSP**: $M_1 \sim$ few hundred GeV, $M_2, |\mu| \gg M_1$. All but the lightest neutralino are effectively inaccessible at the LHC due to their large masses. The NLSP can always decay to $\gamma + \widetilde{G}$, and if it is heavy enough, to $Z + \widetilde{G}$ or $H + \widetilde{G}$.

- **Wino NLSP**: $M_2 \sim$ few hundred GeV, $M_1, |\mu| \gg M_2$. The lightest neutralino and the lightest chargino are nearly degenerate in mass, and are the only two particles to play a role at the LHC. The decays described in the previous bullet point can happen, as well as chargino decays to $W + \widetilde{G}$.

This thesis studied the classic bino NLSP decay $\gamma + \widetilde{G}$.

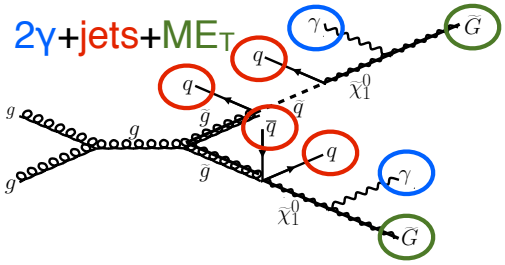

(a) Two gluinos each decay via $\widetilde{\chi}_1^0 \to \gamma\widetilde{G}$.

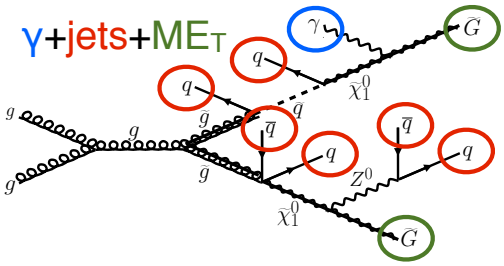

(b) One gluino decays via $\widetilde{\chi}_1^0 \to \gamma\widetilde{G}$, the other via $\widetilde{\chi}_1^0 \to Z(\to q\overline{q})\widetilde{G}$.

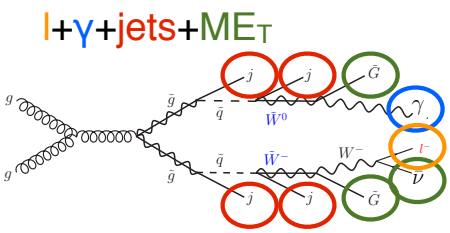

(c) One gluino decays via $\widetilde{\chi}_1^0 \to \gamma\widetilde{G}$, the other via $\chi_1^{\pm} \to W^{\pm}(\to l^{\pm}\nu_l)\widetilde{G}$.

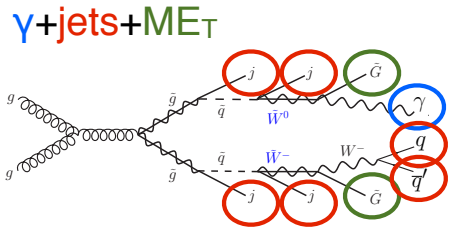

(d) One gluino decays via $\widetilde{\chi}_1^0 \to \gamma\widetilde{G}$, the other via $\chi_1^{\pm} \to W^{\pm}(\to q\overline{q}')\widetilde{G}$.

Figure 1.4: Typical LHC signatures of the bino and wino NLSP scenarios.

Since strong production of SUSY particles dominates over electroweak production at the LHC due to the enhanced gg parton luminosity over the $q\overline{q}$ parton luminosity, early LHC searches are particularly sensitive to light squarks and gluinos. General gauge mediation makes no a priori restrictions on the mass splitting between the strongly interacting sparticles and the weakly interacting sparticles, so models with light squarks and gluinos are viable. In fact, such models could not be probed as well at the Tevatron[4] as they are at the LHC due to the aforementioned parton luminosities.

Typical LHC signatures of the bino and wino NLSP scenarios are shown in Figure 1.4.

[4]Located on the Fermilab site in Batavia, Illinois, the Tevatron was a proton-antiproton collider operating at 1.96 TeV center-of-mass energy. The Tevatron ran from 1987 to 2011 [13].

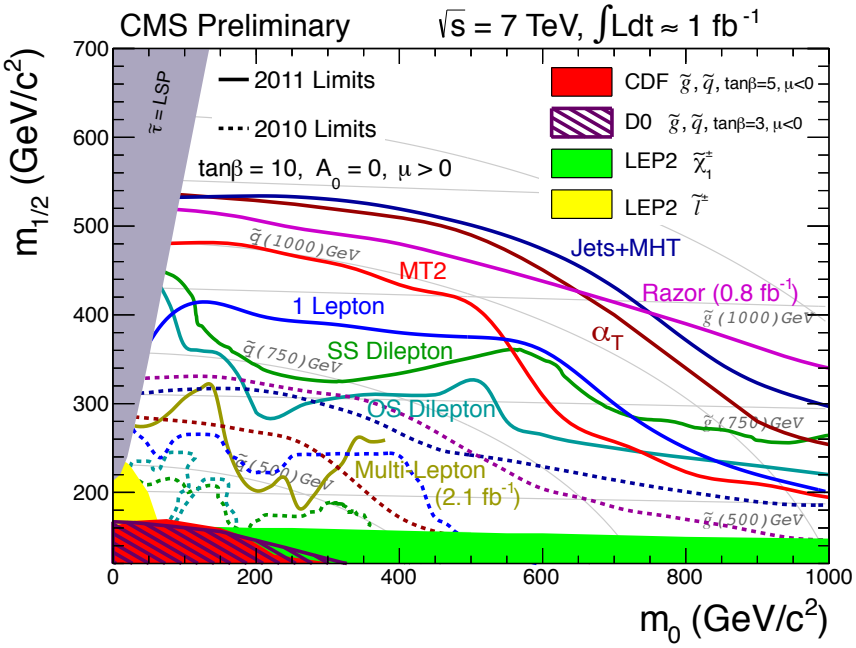

Figure 1.5: CMS limits on mSUGRA with tan $\beta = 10$. The limits set by individual searches are shown as separate colored lines. Solid lines refer to 2011 searches (i.e. using an integrated luminosity of $\sim$1 fb^{-1}), while dashed lines refer to 2010 searches ($\sim$36 pb^{-1}). Reprinted from ref. [15].

1.6 Experimental Status of SUSY

Collider searches for evidence of supersymmetry began in earnest in the 1980s [6] and continue to this day. Most recently, the LHC and Tevatron experiments have set the strictest limits on a variety of SUSY breaking scenarios, including GMSB and mSUGRA.

Figure 1.5 shows the current limits set by the CMS experiment on the mSUGRA model (with tan $\beta = 10$) in the m_0-$m_{1/2}$ plane. (Note that although the plot is truncated at $m_0 = 1000$ GeV/c^2, some searches are sensitive out to $m_0 \sim 2000$ GeV/c^2.) Although the LHC has pushed m_0 above $\sim$1 TeV/c^2 for $m_{1/2}$ up to $\sim$400 GeV/c^2, casting some doubt onto the theory's prospects for solving the hierarchy problem, there is still a sizable chunk of mSUGRA parameter space that is not ruled out by collider experiments. Furthermore, parts of the CMS unexplored regions overlap with areas allowed by astrophysics experiments [14].

Figure 1.6 shows the most up-to-date limit (using 1 fb^{-1} of integrated luminosity collected by the ATLAS experiment [16] at the LHC) on the Snowmass Points and Slopes (SPS) model of mGMSB, dubbed SPS8 [17]. The best limits on a variety of GGM models, from the same ATLAS study, are shown in Figure 1.7. In these models, no assumptions are made about the specific parameters common to many gauge mediation models (e.g. the number of messengers or the relationship between the messenger mass and the SUSY breaking scale). Instead, it is only assumed that the lightest neutralino is light enough to be produced on-shell at the LHC (by setting M_1 and M_2 appropriately, see Sec. 1.5) and that it decays to a gravitino, that the gravitino is extremely relativistic (mass of order eV-keV), and that the gravitino is stable. The one-dimensional scan over SUSY breaking scales in the SPS8 model (in which the full sparticle spectrum is specified by the model parameters) is replaced by a two-dimensional scan over gluino and lightest neutralino mass in the GGM models (in which all sparticles except the gluino, first- and second-generation squarks, and neutralinos are forced to be at $\sim$1.5 TeV/c^2, effectively decoupling them from the dynamics that can be probed with 1 fb^{-1} at a 7 TeV/c pp collider).

In general, the lifetime of the lightest neutralino in GMSB models can take on any value between hundreds of nanometers to a few kilometers depending on the mass of the lightest neutralino and the SUSY breaking scale [18]. The search published in ref. [10] (from which Figs. 1.6 and 1.7 are culled) considers only *prompt* neutralino variants, i.e. with neutralino lifetime short enough that the distance traveled by the neutralino before decay cannot be resolved by the detector. The most recent limits on non-prompt SPS8-style neutralino models were set by the Collider Detector at Fermilab (CDF) collaboration with 570 pb^{-1}, and are shown in Figure 1.8 [11].

Finally, if the gravitino is to make up some or all of the dark matter, constraints on the form of gauge mediation must come from cosmological considerations and astronomical observations. The gravitino in gauge mediation models is usually very

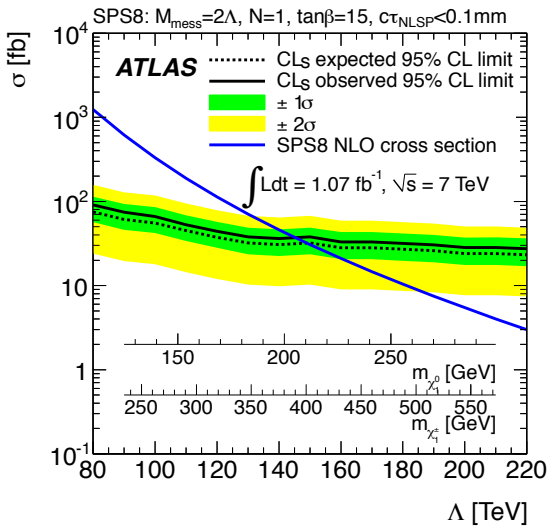

Figure 1.6: ATLAS cross section upper limit on the SPS8 [17] model of mGMSB as a function of SUSY breaking scale Λ, lightest neutralino mass $m_{\widetilde{\chi}_1^0}$, or lightest chargino mass $m_{\widetilde{\chi}_1^\pm}$. Values of Λ, $m_{\widetilde{\chi}_1^0}$, or $m_{\widetilde{\chi}_1^\pm}$ below the intersection point between the blue (predicted SPS8 cross section) and black (observed cross section upper limit) curves are excluded. The model parameters listed above the plot are defined in Secs. 1.4 and 1.5, except for τ_{NLSP}, which is the neutralino lifetime. Reprinted from ref. [10].

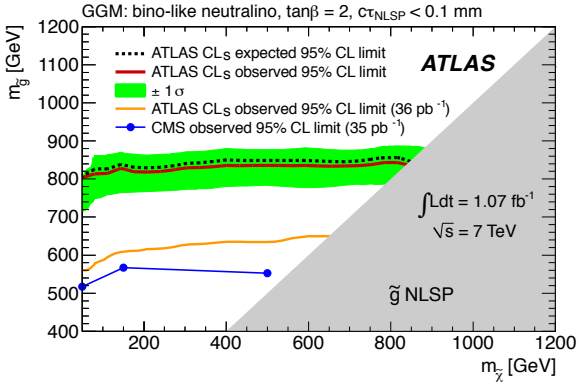

Figure 1.7: ATLAS exclusion contour in the $m_{\widetilde{g}}$-$m_{\widetilde{\chi}_1^0}$ plane. Values of $m_{\widetilde{g}}$-$m_{\widetilde{\chi}_1^0}$ below the red curve are excluded. The gray region is theoretically excluded in the GGM models considered. "Bino-like neutralino" means that $M_2 = 1.5$ TeV/c^2. Reprinted from ref. [10].

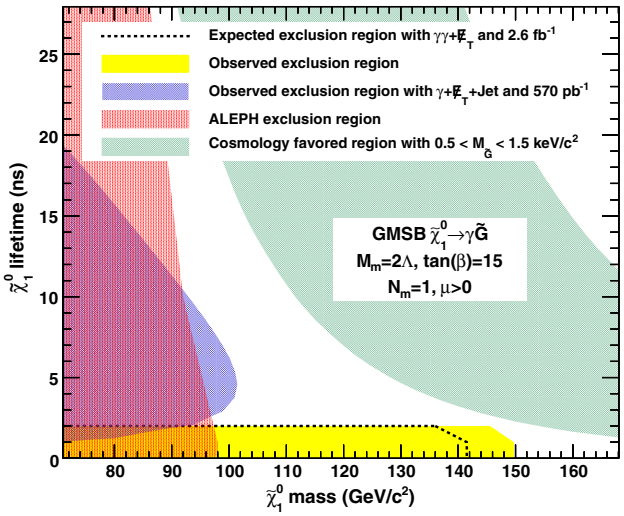

Figure 1.8: CDF exclusion contour in the $\tau_{\widetilde{\chi}_1^0}$-$m_{\widetilde{\chi}_1^0}$ plane, where $\tau_{\widetilde{\chi}_1^0}$ is the lifetime of the neutralino. Reprinted from ref. [11].

light ($\mathcal{O}$(eV-MeV)) because it is proportional to the SUSY breaking scale divided by the Planck mass, and in GMSB the breaking scale is typically only of order a few hundred TeV ([18] and Sec. 1.5). A light, highly relativistic dark matter particle might have been produced, for instance, in the early, radiation-dominated period of the universe [19]. This *warm dark matter* (WDM) may be responsible for all of the dark matter needed to account for galactic structure, or it may share the duties with *cold dark matter* (CDM, weakly interacting particles with masses in the GeV range). In any viable model, the predicted relic density of the dark matter species must match the observed value of $\Omega h^2 \sim 0.1$ [20]. For many GMSB models, this measurement constrains the gravitino mass to the keV range [21]. This constraint, however, does not translate into a very strong bound on the lifetime of the lightest neutralino. Using the following equation (taken from [21]):

$$\tau_{\widetilde{\chi}_1^0} \sim 130\left(\frac{100\ \text{GeV}}{m_{\widetilde{\chi}_1^0}}\right)^5\left(\frac{\sqrt{\langle F\rangle}}{100\ \text{TeV}}\right)^4\ \mu\text{m} \tag{1.24}$$

and applying the gravitino mass constraint $\sqrt{\langle F\rangle} \lesssim 3000$ TeV (cf. the first paragraph of Sec. 1.5 with $m_{\widetilde{G}} \sim$ keV) and $m_{\widetilde{\chi}_1^0} = 100$ GeV, the upper bound on the neutralino

lifetime is 100 meters. For $\sqrt{\langle F \rangle} \sim 100$ TeV, the neutralino lifetime is detectable on collider time scales.

Recently, a lower bound on the WDM particle mass in either pure warm or mixed warm and cold dark matter scenarios was set using observations of the Lyman-α forest. For pure WDM, $m_{\mathrm{WDM}} > 8$ keV, while for some mixed WDM-CDM scenarios, $m_{\mathrm{WDM}} > 1.1$-1.5 keV [19, 22]. These bounds and others have motivated the development of more complicated gauge mediation models [22]. However, rather than focus on a specific GMSB model, of which there are many, the search detailed here is interpreted in a minimally model dependent way. With this approach, the results can be applied to many competing models. The remainder of this thesis is devoted to the experimental details of the search, analysis strategy, and presentation of the results.

Chapter 2

Event Selection

In keeping with the phenomenology described in Sec. 1.5, the candidate GGM events selected in this search consist of two high-E_T photons and a significant momentum imbalance transverse to the beam, indicating the production of an escaping gravitino. This momentum imbalance is usually referred to as *missing transverse energy* and is denoted by the symbol $\not\!\!E_T$.

However, in order to use real CMS data (as opposed to simulation) to derive predictions for the backgrounds to the search, *control samples* distinct from the *candidate* two-photon sample must be collected. These samples consist of different numerical combinations of photons, electrons, and jets, and are explained in more detail in Chapter **??**. Since this search is performed in the high-$\not\!\!E_T$ tail of the $\not\!\!E_T$ distribution, where adequate detector simulation is very difficult, it is advantageous to use *data-driven* background estimates, which capture the true detector response, over numbers derived from simulation.

In the following sections, the reconstruction of photons, electrons, jets, and $\not\!\!E_T$ is explained. Sec. 2.1 begins with an explanation of the high level reconstruction. It is followed by Sec. 2.2, which describes the triggers used to collect the candidate and control samples. Finally, the chapter concludes with a measurement of the photon

identification efficiency in Sec. 2.3.

2.1 Object Reconstruction

This section describes the *offline* object reconstruction, i.e. the reconstruction of particle objects from events that have already been triggered and written to permanent storage, as opposed to the building of trigger objects explained in Secs. **??** and 2.2.

2.1.1 Photons

Uncalibrated EB/EE Hits

Photon reconstruction begins with the ADC count value for each of the 10 recorded time samples per ECAL crystal per trigger. To construct an *uncalibrated hit*, the gain (1, 6, or 12; see Sec. **??**) of each sample is determined and the ADC count value scaled appropriately. The pedestal is estimated from the average of the first three samples, which, for a properly time in hit, should contain no signal. This pedestal value is subtracted from the rest of the samples. Finally, the amplitude of the pulse is reconstructed using a predetermined weight for each sample [23]. The weights correspond to the pulse shape expected from the MGPA and shaping circuit response. The time of the hit is also reconstructed using the ratios between neighboring time samples [24]. A typical ECAL channel pulse shape is shown in Figure 2.1.

Calibrated EB/EE Hits

In the next phase of the photon reconstruction, calibrations are applied to the uncalibrated hits to form *calibrated hits* with energy measured in GeV. Channels are excluded from seeding calibrated hits if

- they are excessively noisy,

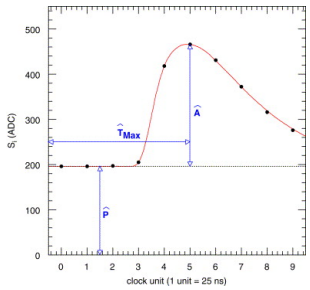

Figure 2.1: Typical ECAL channel pulse shape. $\widehat{P}$ is the pedestal value, $\widehat{A}$ is the pulse amplitude, and $\widehat{T}_{\max}$ is the hit time. The red line is the assumed pulse shape from which the weights are derived. Reprinted from ref. [23].

- they are stuck in fixed gain,
- they are totally dead,
- they have one or more neighboring dead channels, or
- they do not have good trigger primitives (i.e. trigger primitive is missing, saturated, or spike-like).

In addition, no uncalibrated hits that are spike-like are eligible for calibration. The calibrations applied are crystal transparency loss corrections measured continuously by the laser/LED system, energy intercalibrations (relative energy calibration between crystals), absolute scale calibrations between ADC counts and GeV,[1] and time intercalibrations (relative time calibration between crystals).

The ECAL crystals were pre-calibrated before installation in CMS using laboratory light yield and photodetector gain measurements [25]. In addition, some EB and EE crystals were intercalibrated using test beams [26], and all EB crystals were intercalibrated with cosmic ray muons [27]. EE precalibrations were validated with LHC *splash events* in 2009 [27, 28], in which the beam was dumped onto a collimator approximately 150 meters upstream of CMS, causing a spray of muons to enter CMS at

[1]The ADC-GeV scale factors (one for EB and one for EE) are defined such that the sum of fully calibrated and scaled hits in a particular 5 × cluster of crystals (plus the associated energy deposited in ES) is 50 GeV for a 50 GeV incident unconverted photon [31].

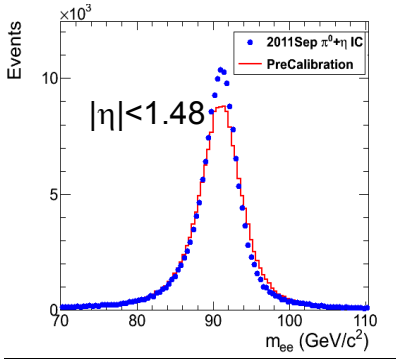

Figure 2.2: Z peak reconstructed using pre-LHC calibration constants (red) or September 2011 π^0/η-derived intercalibration constants (blue). Reprinted from ref. [30].

one endcap and exit at the other. Splash events were also used to derive time intercalibration constants. Before colliding beam operations commenced, the intercalibration precision was estimated to be 0.5%-2.2% in EB and 1%-5% in EE [29].

Three calibration methods were employed once colliding beam operations began:

- ϕ symmetry relative calibration between crystals, exploiting the azimuthal symmetry of CMS
- π^0 and η relative calibration between crystals, using the diphoton decays of these particles
- E/p absolute calibration, comparing the momentum measured in the tracker p to the energy measured in the ECAL E of a sample of electrons from Z decay

By September 2011, the intercalibration precision in EB was measured to be between 0.3% and 1.1% using the π^0/η method [30]. Figure 2.2 shows the improvement in Z reconstruction from pre-LHC calibration constants to the latest π^0/η-derived constants.

Calibrated ES Hits

ES calibrated hits are formed from the three samples read out per sensor. Just as in the case of EB/EE crystals, ES uncalibrated hits gain-adjusted, pedestal-subtracted, and reconstructed using weights. To make a calibrated ES hit, intercalibration constants, angle correction constants, and a MIP-GeV absolute scale factor are applied.

Clustering

After calibrated ECAL hits are formed, they must be clustered into shapes that represent the energy deposit from a single particle. *Basic clusters* are formed around seed hits, defined as a hit that

- has calibrated $E_T > 1(0.18)$ GeV in EB(EE),
- does not originate from a dead channel or one with faulty hardware,
- is not poorly calibrated,
- was reconstructed with the standard algorithm (i.e. not a special recovery algorithm for channels with subpar data integrity),
- is not saturated,
- is not spike-like, and
- is in time (EB).

EB basic clusters are formed around the seeds via the *hybrid* algorithm, while EE basic clusters are formed with the *multi5x5* algorithm [32]. In addition to non-radiating electrons and unconverted photons, both algorithms are designed to also recover all of the energy associated with electron bremsstrahlung deposits and photon conversions. The geometry of the CMS magnetic field means that bremsstrahlung and conversions will tend to spread the shower out in ϕ, not η. Both algorithms work by forming

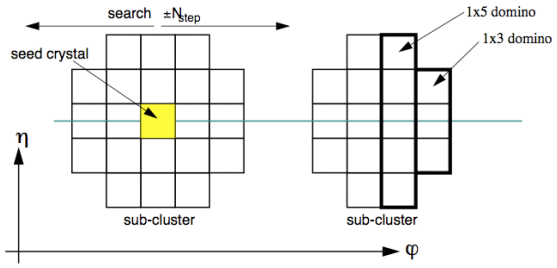

Figure 2.3: Hybrid algorithm in EB. The shower extent is essentially constant in η, but spreads out in ϕ as the two sub-clusters (or basic clusters) are grouped into the same supercluster. Reprinted from ref. [32].

basic clusters around seeds, then combining the basic clusters into *superclusters* (SC) by searching in a window extended in the ϕ direction for all basic clusters consistent with bremsstrahlung radiation from the primary electron, or with a photon conversion. Figure 2.3 illustrates the hybrid algorithm in EB. In EE, the energy deposited in ES must also be added into the total clustered energy sum.

Supercluster Corrections

The total clustered ECAL energy is defined as

$$E = F \times \sum_{i=1}^{n_{\text{crystal}}} G \times c_i \times A_i \tag{2.1}$$

where G is the ADC-GeV or MIP-GeV scale factor, c_i are the intercalibration constants, A_i is the uncalibrated hit amplitude in ADC counts, and F is SC correction factor. G and c_i were explained in Secs. 2.1.1 and 2.1.1. F is a product of three factors for hybrid SCs (two for multi5x5 SCs) [32]:

1. $C_{EB}(\eta|)$, which compensates for lateral energy leakage due to the crystal off-pointing in EB. These corrections are taken from MC simulation [32] and were confirmed in test beams [26].

2. $f(\text{brem})$, which corrects for the biases in the clustering algorithms for showers

characterized by differing amounts of bremsstrahlung. These corrections are taken from MC simulation [32].

3. Residual correction $f(E_T, \eta)$, due to the variation in η of detector material traversed by a primary electron or photon, and to any residual E_T dependence of the reconstruction. These corrections are determined from $Z \to ee$ data samples.

From Supercluster to Photon

The CMS photon object is any SC with $E_T > 10$ GeV and $H/E < 0.5$, unless the SC $E_T > 100$ GeV, in which case the H/E requirement is dropped. H/E is defined as the ratio of energy in the HCAL in a 0.15 cone around the SC centroid, directly behind the SC, to the SC energy. SCs with $R9 > 0.94(0.95)$ in EB(EE), where $R9$ is defined as $E_{3\times3}/E_{SC}$, are the best calibrated and most accurate type of electromagnetic shower. Therefore, for these objects, the photon energy is defined as the energy sum of the fully calibrated hits in the central 5×5 cluster around the seed (with $C_{EB}(\eta)$ applied for EB photons). For all other SCs, the photon energy is equal to the fully corrected SC energy (cf. Sec. 2.1.1).

In this search, candidate photons and *fake photons* (f, "fakes") are further selected according to the criteria listed in Table 2.1. Fakes are used in the determination of the QCD background, as explained in Chapter **??**. I_{comb} is defined as

$$I_{\text{comb}} = I_{\text{ECAL}} - 0.0792\rho + I_{\text{HCAL}} - 0.0252\rho + I_{\text{track}} \tag{2.2}$$

where I_{ECAL}, I_{HCAL}, and I_{track} are E_T sums in the annular regions defined in Figure 2.4 and ρ is the average pileup energy density in the calorimeters (per unit $\eta \cdot \phi$) as measured with the Fastjet algorithm [33, 34]. Figure 2.5 shows the ρ distribution

for a sample of events with at least two 25 GeV EM objects passing the $|\eta|$, H/E, and $R9$ requirements in Table **??**, and passing the trigger requirements in Table **??**, representing the full 2011 dataset. Since average ρ is $\sim$ 5 GeV, and there is a long tail above this average value, it is necessary to subtract pileup energy from the ECAL and HCAL isolation cones to recover otherwise clean photons in events with large pileup. The ECAL and HCAL *effective areas* of 0.0792 and 0.0252, respectively, are calculated by fitting the average ECAL or HCAL isolation energy vs. ρ in a sample of $Z \to ee$ events to a straight line. The slope of the line—which has the units of $\eta \cdot \phi$, or area—is the effective area.

A "pixel seed" is defined as a hit in the pixel detector consistent with a track extrapolated from the position of the ECAL SC back to the primary vertex. Real photons, having no charge and therefore no bending in the magnetic field, should not have a pixel seed.

Table 2.1: Selection criteria for photons and fakes.

Variable	Cut (γ)	Cut (f)
SC $\lvert\eta\rvert$	< 1.4442	< 1.4442
H/E	< 0.05	< 0.05
$R9$	< 1	< 1
Has pixel seed	No	No
I_{comb}	< 6 GeV	≥ 6 and < 20 GeV

2.1.2 Electrons

Electrons are reconstructed identically to photons, except that in the electron case the presence of a pixel seed is enforced, rather than vetoed.[2] Photons and electrons are defined by very similar criteria so that $Z \to ee$ events can be used to model the QCD background in the two-photon sample without introducing any bias in the

[2]In many CMS analyses, electrons are reconstructed very differently from photons. In particular, a special tracking algorithm [35] is used to best follow a radiating electron. However, in this analysis, the electron tracking is not used.

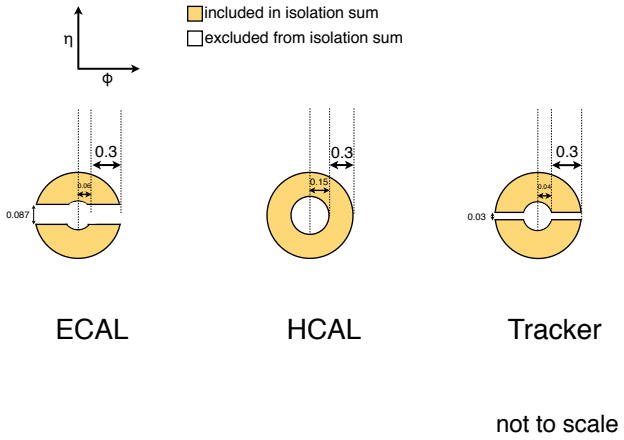

Figure 2.4: ECAL, HCAL, and track Isolation cones.

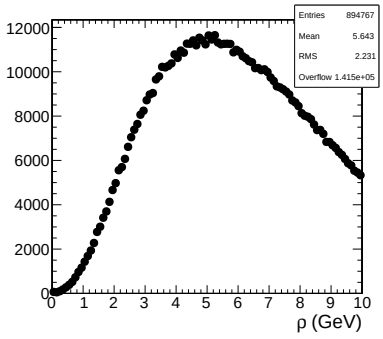

Figure 2.5: ρ distribution for a sample of events with at least two 25 GeV EM objects passing the $|\eta|$, H/E, and $R9$ requirements in Table **??**, and passing the trigger requirements in Table **??**. This sample covers the full 2011 dataset.

electron energy measurement (cf. Sec. **??**).

2.1.3 Jets and Missing Transverse Energy

2.2 HLT

From the objects described in Sec. 2.1, four samples of events are formed:

- $\gamma\gamma$ candidate sample, in which the two highest E_T objects are photons,
- $e\gamma$ control sample, in which the two highest E_T objects are one electron and one photon,
- ee control sample, in which the two highest E_T objects are electrons, and
- $\not{f}\not{f}$ control sample, in which the two highest E_T objects are fakes.

In all samples, the leading EM object is required to have $E_T > 40$ GeV, while the trailing EM object is required to have $E_T > 25$ GeV. The high level triggers used to select the four samples, by run range, are listed in Table 2.2. No trigger is prescaled.

Each piece of the HLT path name is defined as follows.

- "Photon": Energy deposit in the ECAL that fired an L1 trigger (cf. Sec. **??**). For Photon26_IsoVL_Photon18, the L1 seed E_T threshold is 12 GeV, while for all other triggers in Table 2.2 it is 20 GeV.
- Integer following the word "Photon": E_T threshold in GeV for offline reconstructed photon, using the full photon reconstruction of Sec. 2.1.1 minus the laser calibrations and assuming the primary vertex at (0, 0, 0).
- "CaloIdL": For EB photons, $H/E < 0.15$ and $\sigma_{i\eta i\eta} < 0.014$.
- "IsoVL": $I_{\mathrm{ECAL}} < 0.012E_T + 6$ GeV, $I_{\mathrm{HCAL}} < 0.005E_T + 4$ GeV, and $I_{\mathrm{track}} < 0.002E_T + 4$ GeV.

Table 2.2: HLT paths triggered by the $\gamma\gamma$, $e\gamma$, ee, and ff samples, by run range. No triggers are prescaled.

Run range	$\gamma\gamma$	$e\gamma$	ee	ff
160404-161215	Photon26_ IsoVL_ Photon18	Photon26_ IsoVL_ Photon18	Photon26_ IsoVL_ Photon18	Photon26_ IsoVL_ Photon18
161216-166346	Photon36_ CaloIdL_ Photon22_ CaloIdL	Photon36_ CaloIdL_ Photon22_ CaloIdL	Photon36_ CaloIdL_ Photon22_ CaloIdL	Photon36_ CaloIdL_ Photon22_ CaloIdL
166347-180252	Photon36_ CaloIdL_ IsoVL_ Photon22_ CaloIdL_ IsoVL	Photon36_ CaloIdL_ IsoVL_ Photon22_ CaloIdL_ IsoVL	Photon36_ CaloIdL_ IsoVL_ Photon22_ CaloIdL_ IsoVL Photon36_ CaloIdL_ IsoVL_ Photon22_ R9Id Photon36_ R9Id_ Photon22_ CaloIdL_ IsoVL Photon36_ R9Id_ Photon22_ R9Id	Photon36_ CaloIdL_ IsoVL_ Photon22_ CaloIdL_ IsoVL Photon36_ CaloIdL_ IsoVL_ Photon22_ R9Id Photon36_ R9Id_ Photon22_ CaloIdL_ IsoVL Photon36_ R9Id_ Photon22_ R9Id

- "R9Id": $R9 > 0.8$.

In addition, the versions of HLT_Photon26_IsoVL_Photon18 and Photon36_CaloIdL_Photon22_CaloIdL that were active during runs 160404-163268 included a cut $E_{\max}/E_{5\times5} < 0.98$ for spike rejection. $E_{\max}$ is the energy in the highest energy crystal of the EM cluster and $E_{5\times5}$ is the energy in the 5×5 crystal matrix around the seed crystal. For runs after 163268, Swiss cross spike rejection of individual crystals from HLT quantities was performed (cf. Sec. **??**). All information about the evolution of the CMS HLT settings can be found in the HLT configuration browser at `http://j2eeps.cern.ch/cms-project-confdb-hltdev/browser/`.

As an example of the naming convention just described, the HLT path Photon36_CaloIdL_IsoVL_Photon22_R9Id is fired if one photon is found with $E_T > 36$ GeV passing the CaloIdL and IsoVL requirements, and another is found with $E_T > 22$ GeV passing the R9Id requirement.

2.3 Photon Identification Efficiency

Lorum ipsum fuck Republicans.

Bibliography

[1] S.L. Glashow, J. Iliopoulis, and L. Maiani, *Phys. Rev. D* **2** (1970) 1285; S.L. Glashow, *Nucl. Phys.* **22(4)** (1961) 579; J. Goldstone, A. Salam, and S. Weinberg, *Phys. Rev.* **127** (1962) 965; S. Weinberg, *Phys. Rev. Lett.* **19** (1967) 1264; A. Salam and J.C. Ward, *Phys. Lett.* **13(2)** (1964) 168.

[2] M. Gell-Mann, *Phys. Lett.* **8** (1964) 214; G. Zweig, *CERN* **8419/TH. 412** (1964) (unpublished).

[3] J. Drees, *Int. J. Mod. Phys.* **A17** (2002) 3259.

[4] P.W. Higgs, *Phys. Lett.* **12(2)** (1964) 132; P.W. Higgs, *Phys. Rev. Lett.* **13** (1964) 508; P.W. Higgs, *Phys. Rev.* **145** (1966) 1156.

[5] I. Aitchison, *Supersymmetry in Particle Physics: An Elementary Introduction* (Cambridge University Press, Cambridge 2007), p. 4.

[6] E. Fernandez et al., *Phys. Rev. Lett.* **54** (1985) 1118; E. Fernandex et al., *Phys. Rev.* **D35** (1987) 374; D. Decamp et al., *Phys. Lett.* **B237(2)** (1990) 291; F. Abe et al., *Phys. Rev. Lett.* **75** (1995) 613; S. Abachi et al., *Phys. Rev. Lett.* **75** (1995) 618; G. Alexander et al., *Phys. Lett.* **B377(4)** (1996) 273; S. Aid et al., *Z. Phys.* **C71(2)** (1996) 211; S. Aid et al., *Phys. Lett.* **B380(3-4** (1996) 461; B. Aubert et al., *Phys. Rev. Lett.* **95** (2005) 041802.

[7] M. Dine and W. Fischler, *Phys. Lett.* **B110** (1982) 227; C.R. Nappi and B.A. Ovrut, *Phys. Lett.* **B113** (1982) 175; L. Alvarez-Gaumé, M. Claudson, and M.B. Wise, *Nucl. Phys.* **B207** (1982) 96; M. Dine and A.E. Nelson, *Phys. Rev.* **D48** (1993) 1277; M. Dine, A.E. Nelson, and Y. Shirman, *Phys. Rev.* **D51** (1995) 1362; M. Dine, A.E. Nelson, Y. Nir, and Y. Shirman, *Phys. Rev.* **D53** (1996) 2658.

[8] A.H. Chamseddine, R. Arnowitt, and P. Nath, *Phys. Rev. Lett.* **49** (1982) 970; R. Barbieri, S. Ferrara, and C.A. Savoy, *Phys. Lett.* **B119** (1982) 343; L.E. Ibáñez, *Phys. Lett.* **B118** (1982) 73; L.J. Hall, J.D. Lykken, and S. Weinberg, *Phys. Rev.* **D27** (1983) 2359; N. Ohta, *Prog. Theor. Phys.* **70** (1983) 542; J. Ellis, D.V. Nanopoulos, and K. Tamvakis, *Phys. Lett.* **B121** (1983) 123; L. Alvarez-Gaumé, J. Polchinski, and M. Wise, *Nucl. Phys.* **B221** (1983) 495.

[9] P. Meade, N. Seiberg, and D. Shih, *Progr. Theor. Phys. Suppl.* **177** (2009) 143.

[10] G. Aad et al., *CERN-PH-EP-2011-160* (2011).

[11] T. Aaltonen et al., *Phys. Rev. Lett.* **104** (2010) 011801.

[12] CMS Collaboration, *CMS-PAS-SUS-11-009* (2011).

[13] `http://en.wikipedia.org/wiki/Tevatron`.

[14] O. Buchmueller et al., *CERN-PH-TH/2011-220* (2011).

[15] `https://twiki.cern.ch/twiki/bin/view/CMSPublic/PhysicsResultsSUS`.

[16] G. Aad et al., *JINST* **3** (2008) S08003.

[17] B.C. Allanach et al., *Eur. Phys. J.* **C25** (2002) 113.

[18] S. P. Martin, *A Supersymmetry Primer* **v4** (2006) 86. arXiv:hep-ph/9709356.

[19] A. Boyarsky, J. Lesgourgues, O. Ruchayskiy, and M. Viel, *CERN-PH-TH/2008-234* (2009).

[20] E. Komatsu et al., *Astrophys. J. Suppl. Ser.* **180** (2009) 330.

[21] C.-H. Chen and J.F. Gunion, *Physical Review* **D58** (1998) 075005.

[22] F. Staub, W. Porod, J. Niemeyer, *JHEP* **1001** (2010) 058.

[23] R. Brunelière, *Nucl. Instr. Meth. Res.* **A572** (2007) 33.

[24] S. Chatrchyan et al. (CMS Collaboration), *JINST* **5** (2010) T03011.

[25] P. Adzic et al. (CMS Electromagnetic Calorimeter Group), *Eur. Phys. J.* **C44S2** (2006) 1.

[26] P. Adzic et al. (CMS Electromagnetic Calorimeter Group), *JINST* **3** (2008) P10007.

[27] M. Malberti, *Nuc. Sci. Symposium Conference Record NSS/MIC IEEE* (2009) 2264.

[28] S. Chatrchyan et al. (CMS Collaboration), *JINST* **5** (2010) T03010.

[29] R. Paramatti, *J. Phys. Conf. Ser.* **293** (2011) 012045.

[30] Y. Yang, `http://www.hep.caltech.edu/cms/posters/Pi0Poster_CMSWeekDec2011.pdf` (2011).

[31] P. Meridiani and C. Seez, *CMS IN-2011/002* (2011).

[32] M. Anderson, A. Askew, A.F. Barfuss, D. Evans, F.Ferri, K. Kaadze, Y. Maravin, P. Meridiani, and C. Seez, *CMS IN-2010/008* (2010).

[33] M. Cacciari, *LPTHE-P06-04* (2006).

[34] M. Cacciari, G.P. Salam, and G. Soyez, *CERN-PH-TH-2011-297* (2011).

[35] W. Adam, R. Früwirth, A. Strandlie, and T. Todorov, *J. Phys.* **G31** No. 9 (2005).

[36] S. Chatrchyan et al., *JINST* **6** (2011) P11002.